Quantification of sub-millimeter displacements caused by sinkholes, using distributed optical fiber sensors

Edouard Buchoud, Valeriu Vrabie, Jerome I. Mars, Guy d'Urso, Alexandre Girard, Sylvain Blairon, Jean-Marie Henault

Quantification of sub-millimeter displacements by distributed optical fiber sensors

E. Buchoud, V. Vrabie, J.I. Mars, G. D'Urso, A. Girard, S. Blairon, and J-M. Henault

***Abstract*—The estimation of sinkhole-induced ground displacement is an important issue for monitoring soil structures. Distributed optical fiber sensors composed of an interrogator based on scattering effects in an optical fiber cable sensing element can be used to assess ground displacement. These sensors provide longitudinal strain measurements of the soil structure. This article proposes a methodology that enables estimation of displacement fields in the soil structure when a sinkhole appears. It also exposes an experiment which was carried out to create an artificial sinkhole instrumented by optical fiber sensors. This is the first time that those sensors are used to provide sub-millimeter vertical displacements. The first step of the methodology is to model the ground displacement under two-dimensional conditions. The longitudinal strain measured by a distributed optical fiber sensor can thus be linked to the displacement of the structure. This model is described by those parameters: the spatial extent of the displacement signature; a coefficient that depends on the interface between the optical fiber cable and the soil; the depth of the sinkhole; and the maximal vertical displacement. The second step consists of the estimation of each parameter independently. The spatial extension is given by fitting the measured strain signature with the empirical model. The depth of the sinkhole can be determined by measurement of the spatial extension of the ground-displacement profile at several observation depths in the structure. Finally, the vertical maximal displacement is furnished with high precision.**

***Index Terms*—Monitoring, Brillouin scattering, Optical fiber measurement application, signal processing, displacement measurement.**

I. Introduction

The durability of civil infrastructures is a crucial issue that can have major economic, social, and environmental impacts. In civil engineering, many aging infrastructures can become vulnerable in terms of their stability due to internal erosion, climatic conditions, and other natural phenomena. Infrastructure owners and users can face difficult challenges, such as optimization of maintenance and extension of service life. In this context, as the major owner of dykes and dams in France, Electricité de France (EDF) is in charge of the monitoring of these soil structures. The stability of dykes can be threatened when internal erosion occurs; e.g., water infiltration into the core of the dyke can induce ground displacement at the interface of the two soil strata. The main defective phenomena are sinkholes, piping effects, and underground cavities, and if these appear, they can induce severe consequences on the stability of the structure [1]. To prevent failure of such structures, displacement induced by these phenomena have to be detected, localized, and quantified with precision, to provide efficient monitoring.

Structural health monitoring is considered a key procedure in industrial processes, because it provides real-time diagnosis of the state of wear/ damage of a structure. Conventional structural health monitoring methods to detect and localize ground displacement are usually based on visual inspections of sites or point-to-point measurements of several internal parameters, such as pressure, flow, temperature, and strain. These methods are based on localized sensors that allow access only to the local mechanical and thermal behavior of the structure. Self-potential and resistivity methods can provide efficient measurements [2-5], although these methods are still manual and require careful placement and use of electronic equipment at the site.

As a complement to conventional sensors, distributed optical fiber sensors (DOFS) have gained significant interest for the monitoring of large structures, due to their robustness, immunity to electromagnetic interference, and deployment in harsh environments. For concrete structures [6-8] and tunnel and dyke monitoring [9-12] in the oil and gas industries [13], DOFS are widely used to detect and localize leakages or displacement, through advanced analysis of the distributed temperature or strain measurements. DOFS allow continuous measurements of strain and/or temperature over kilometers, with the classical trade-off between spatial resolution and distance. Technologies based on Rayleigh scattering, such as the Luna optical backscatter reflectometer (OBR 1600), have spatial resolution of 1 cm, with measurement distance <100 m [14]. In contrast, a Brillouin optical time-domain analyzer (B-OTDA), such as the Omnisens DiTest STA-R, provides surveys at up to 30 km, but with a 40 cm limited spatial resolution [15].

Over the last decade, significant efforts have been invested in fiber optic installations, as well as in data interpretation for structural health monitoring [8]-[13]-[17]. Metrological performances of B-OTDAs have been enhanced by post-treatment algorithms for data handling [14]-[16]-[18]-[19] and improvements in spatial resolution, to detect strain induced by ground displacement with centimeter resolution [14]-[18]. As the strain measurements are influenced by thermal changes, temperature compensation problems have also been assessed to estimate the irreversible strain in optical fibers [20]. The aim of this study was to establish a methodology for interpretation of strain signatures provided by DOFS, which is the final, but crucial, step for the quantification of displacement.

This paper addresses the problem of quantification of displacement induced by sinkholes through careful interpretation of DOFS strain signatures. As these signatures are related to the longitudinal component of the strain tensor in the optical fiber, the main hurdle is to establish the relationship

between the longitudinal strain signature and the ground displacement that is induced by sinkhole formation. Based on the assumption that sinkhole formation is close to tunneling, this article was inspired by previous studies in the tunneling domain that have indicated that vertical displacements induced by man-made underground tunnels can be modeled according to empirical and/or analytical laws [21]-[22]. Under simple strain conditions, empirical laws have few parameters related to the shape of the displacement signature, including inflection points, depth, and vertical maximal displacement. The analytical models that describe displacement profiles indicate that the results have many parameters that depend on the geometry of the structure and the soil coefficients, and their computation can be particularly time consuming [22]. As DOFS allow the measurement of the longitudinal strain in an optical fiber, a link between the displacement models and the strain measurements can be defined [23]. Thus, in the tunnel domain, it is possible to optimize the shape parameters to estimate the vertical displacement if the depth of the man-made cavity is known. In the case of sinkhole formation, the depth of the natural cavity has to be estimated first, then the vertical displacement can be calculated.

We propose here a methodology based on a new model of the longitudinal strain signature provided by DOFS. It allows general shapes to be covered, thus providing an accurate description of the displacement field in the soil. Based on several DOFS strain measurements from the same event, the evolution of the shape according to the depth of the observation can be expressed, which independently allows the estimation of the parameters of the model.

To validate this methodology, an experiment was carried out to create an artificial sinkhole through a trap-door system, with 1.5 m of sandy soil above a trap-door. Two observation depths were installed with an industrialized optical fiber coupled with the Rayleigh and Brillouin scattering-based sensors, which provided longitudinal strain measurements. The results show that this proposed methodology means that the DOFS can be used to precisely estimate sub-millimeter vertical displacement.

This article is composed of three sections. The first section presents the relationships that describe the signature of the displacement of the ground in terms of tunnel formation. As sinkholes have general forms, we propose an alternative model to predict these. The second section analyses the link between the strain measurements and the parameters of the proposed model. Based on this, a new methodology that allows the estimation of the cavity depth and the induced vertical displacement is presented. The third section presents a field investigation in which the methodology is applied and validated. We show through a real dataset that the proposed methodology can provide quantification of sub-millimeter vertical displacement in the soil. A discussion follows about how the use of the post-processed B-OTDA strain measurements instead of Rayleigh strain measurements enables precise estimation of vertical displacement.

II. GROUND MOVEMENT INDUCED BY SINKHOLES

A. Ground-displacement models

Several empirical and analytical models have been developed to estimate ground displacement of buildings and pipelines induced by tunnel construction [21]-[22]-[24]. The profile of the ground once it has settled following the displacement (i.e., the ground settlement profile) is associated with a predefined shape function in the empirical models, which results from the solution of the continuum that governs the equations in the analytical models. The advantage of the empirical model is the use of few shape parameters. The current study focuses on the two-dimensional empirical models (under simple strain conditions) to predict the ground displacement signature induced by a natural underground cavity (Fig. 1). In the specific case of the sinkhole, the unknown parameters lie in the localization in space of the cavity: the depth z_s and the abscissa x_s in the structure; the induced maximal ground settlement $s_{max}(z)$; and the longitudinal extension of profile i_x. Several curves have been proposed to fit the observed ground settlement profile as a consequence of tunneling. The first one was proposed by Peck *et al.* [21]. They fit the shape to a classical Gaussian curve with the two degrees of freedom represented by i_x and s_{max}. Later, several studies [24]-[25] showed that this Gaussian curve is limiting for the full description of the signature of the vertical displacement. Other functions have thus been suggested (Table I): the modified Gaussian of Jacobsz *et al.* [26]; the generalized Lorentz function of Celestino *et al.* [24]; and the particular Lorentz function of Vorster *et al.* [25]. These last two (the Celestino and Vorster's models) with two degrees of freedom increase the flexibility of the shape. It has also been shown that the more parameters included, the more complicated the interpretation of the model with respect to the estimation of the ground displacement [27]. While the shape of a tunnel is relatively round or oval, a sinkhole might have several *shapes* within its structure, and might not produce a symmetric displacement signature. Therefore, to be more realistic, we introduce a new model here that provides for more general shapes of displacement in the structure. This model combines the two main shapes considered to be the state of the art [23], as a Gaussian function with a Lorentzian function, which is also known as the pseudo-Voigt function, and is given by (1):

$$u_z(x,z) = s_{\max}(z) \times \left(\frac{c(z)}{1-\rho^2} + (1-c(z)) \times e^{-\frac{1}{2}\times\frac{(x-x_s)^2}{\lambda(z)^2}}\right) \quad (1).$$

with $\rho = (x - x_s)/\Gamma(z)$. The displacement pattern $u_z(x,z)$ is ruled by three degrees of freedom: c, the ratio between the Gaussian and Lorentzian parts, Γ and λ, which are their widths,

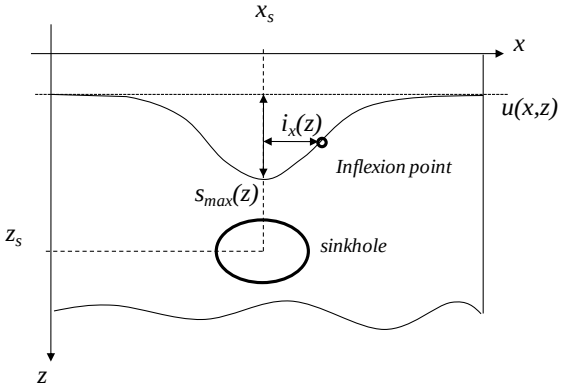

Fig. 1. Ground settlement trough, *u(x,z)*, induced by a sinkhole.

TABLE I
EMPIRICAL MODELS AND CHARACTERISTICS USED TO DESCRIBE THE GROUND SETTLEMENT PROFILE

Equation of curve $u_z(x,z)$	Additional details	Validity domain	Reference
$u_z(x,z) = s_{max}(z) \times e^{-\frac{1}{2}\frac{(x-x_s)^2}{i_x(z)^2}}$	$u_z(i_x,z) = 0.606 \times s_{max}(z)$	$i_x \in \mathbb{R}_+^*$	[21]
$u_z(x,z) = \frac{s_{max}(z)}{1+(\lvert x-x_s\rvert/a)^b}$	$i_x(z) = a \times B$; $B = (\frac{b-1}{b+1})^{1/b}$	$\{b,a\} \in \mathbb{R}_+^*$	[22]
$u_z(x,z) = s_{max}(z) \times e^{-\frac{1}{3}\times\left(\frac{\lvert x-x_s\rvert}{i_x(z)}\right)^{1.5}}$	$u_z(i_x,z) = 0.717 \times s_{max}(z)$	$i_x \in \mathbb{R}_+^*$	[26]
$u_z(x,z) = \frac{q \times s_{max}(z)}{(q-1)+e^{\mu\cdot((x-x_s)/i_x(z))^2}}$	$q = e^{\mu} \times \frac{2\mu-1}{2\mu+1} + 1$	$\{i_x,\mu\} \in \mathbb{R}_+^*$	[25]

respectively, both of which lie between 0 and 1. When c = 0 or 1, the displacement profile is proportional to a Gaussian or a Lorentzian distribution, respectively.

B. Link between measured strain and displacement

1) Longitudinal strain measurement

Distributed optical fiber sensors are composed of the sensing element, the optical fiber cable, and an opto-electronic device, known as the interrogator. A light impulse is launched into the fiber and is backscattered to the analyzer of the interrogator. The Brillouin and Rayleigh scattering phenomena are sensitive to the strain and temperature of the silica in the fiber. The measurement of the sensing element can be localized at a point 'x', due to the time-of-flight of the impulse in the fiber.

The Rayleigh scattering device is commonly used in laboratory experiments because of its centimeter spatial resolution and the associated high resolution of ±5 µm/m [15], although this device is not appropriate to monitor large soil structures as its maximum gauge length is limited to 100 m. Using a B-OTDA, the Brillouin scattering allows the measurement of the strain of the sensing element over kilometers, but with a minimum base length integration, w, of 1 m. As the information is averaged into this base, the minimal spatial resolution is 40 cm. This limitation arises from the physical length of the light impulse [16].

The longitudinal strain measurement with DOFS relies on the relationship between the frequency shift, $\Delta\nu_f(x,z)$, the relative strain, $\varepsilon_f(x,z)$, and the relative temperature, $\Delta T_f(x,z)$, in the optical fiber, as measured for two different states: the reference state, when the fiber is in its initial position; and the stressed state [28], such that:

$$\Delta\nu_f(x,z) = C_\varepsilon \times \varepsilon_f(x,z) + C_T \times \Delta T_f(x,z) \quad (2),$$

where C_ε and C_T are calibration coefficients that are related to the strain and temperature, depending on the optical fiber. For standard optical fiber cables operating at λ_0 = 1550 nm, typical values of C_ε and C_T for B-OTDA scattering-based sensors are 0.05 MHz/µε and 1.0 MHz/°C, respectively [28], and for Rayleigh scattering-based sensors, -0.15 GHz/µε and -1.25 GHz/°C, respectively [15].

If the optical fiber cable is laid along the x-axis of the studied structure [8] [29], the relationship between the measured strain in the fiber $\varepsilon_f(x,z)$, and the longitudinal strain in the structure $\varepsilon_{xx}(x,z)$, is given by:

$$\varepsilon_f(x,z) = \varepsilon_{xx}(x,z) * F_{coating}(x,z) * \Pi_{int}(x) \quad (3),$$

where $F_{coating}$ is the system soil–optical fiber cable mechanical transfer function, which merges the influence of the interactions between the soil, the cable, and the variation of the Young modulus in the cable. Here, $\Pi_{int}(x)$ represents the influence of the spatial resolution of the interrogator, which can be seen as a weighting function [8]-[14]-[30], and "*" is the convolution product. A methodology based on advanced signal processing techniques allows the estimation of the strain signature from the B-OTDA spectral data with centimeter spatial resolution [14]. In this way, the impact of the spatial resolution of the interrogator on the strain signature can be ignored. This assumption for the use of the B-OTDA measurements is discussed in the next sections.

Only the mechanical transfer function of the cable influences the measured strain in the fiber. Henault *et al.* [8] defined a methodology to experimentally estimate $F_{coating}(x,z)$ in concrete structures by applying an impulse disturbance (such that $\tilde{F}_{coating}(x,z) = \varepsilon_f(x,z)$) and recording the strain measurement with centimeter spatial resolution using a Rayleigh scattering device. In large soil structures, local constraints are less important than in concrete structures, because of the small displacement in soil with larger dimensions. These phenomena will involve a long section of the cable, with the effect of the coating of the cable on the shape of the signature being negligible, although not for its amplitude. This hypothesis indicates that the longitudinal strain measured by the sensor is proportional to the longitudinal strain in the structure in the local area around the cable. The influence of the mechanical transfer function comes down to a multiplicative coefficient, γ, that allows (3) to be expressed as:

$$\varepsilon_f(x,z) \cong \gamma \times \varepsilon_{xx}(x,z) \quad (4).$$

2) Longitudinal strain into the structure

The strain tensor, **E**, in the soil, which is expressed as $\boldsymbol{E} = \frac{1}{2} \times (\nabla \boldsymbol{u} + (\nabla \boldsymbol{u})^t)$, where $\nabla = \frac{\partial.}{\partial x} + \frac{\partial.}{\partial y} + \frac{\partial.}{\partial z}$, depends on the soil displacement vector, **u**. The longitudinal strain in the soil is defined as [10]:

$$\varepsilon_{xx}(x,z) = \frac{\partial u_x(x,z)}{\partial x} \quad (5),$$

where $u_x(x,z)$ is the longitudinal (horizontal) displacement at the depth of the optical fiber cable. It is commonly assumed that the longitudinal displacement profile, $u_x(x,z)$, is linked to the vertical one, $u_z(x,z)$ [31], such that:

$$u_x(x,z) = -\frac{n\times(x-x_s)}{\Delta z} \times u_z(x,z) \quad (6),$$

where *n* is a dimensionless parameter that is linked to the soil stiffness. The value of *n* can be found through laboratory tests, and it lies between 0.4 and 0.9 for sand and soft clay, respectively [23]. $\Delta z = z - z_s$ is the vertical distance between the center of the underground cavity and the optical fiber cable. The longitudinal strain in the soil can be expressed through (1), (3), (5), and (6) as:

$$\varepsilon_f(x,z) = -A(z) \times \left(\frac{u_z(x,z)}{s_{max}(z)} + c(z) \times \frac{2\times\rho^2}{(1-\rho^2)^2} - (1-c(z)) \times \left(\frac{x-x_s}{\lambda(z)}\right)^2 \times e^{-\frac{1}{2}\times\left(\frac{x-x_s}{\lambda(z)}\right)^2}\right) \quad (7),$$

with $A(z) = \frac{n_f \times s_{max}(z)}{\Delta z}$ As we made the assumption that $\varepsilon_f(x) \cong \gamma \times \varepsilon_{xx}(x)$, we introduce the parameter $n_f = \gamma \times n$, which is here dependent on the coating of the cable. When $x = x_s$, the longitudinal strain, $\varepsilon_f(x = x_s, z) = -n_f \times s_{max}(z)/\Delta z$, is denoted as *A(z)*, and it corresponds to the minimum value of the strain measurement.

III. Quantification of the Displacement

A. Estimation of the model parameter

Distributed optical fiber sensors can provide distributed strain measurements with centimeter spatial resolution, either through the interrogator (i.e., the Rayleigh device) or through advanced signal processing of the Brillouin spectra (i.e., the B-OTDA device) [14], so that it is possible to precisely compare the modeled strain profile and the measured strain profile. The parameters of the model in (7) can be estimated by minimizing the quadratic error, such that:

$$\{s_{max}, n_f, \Delta z, i_x, c, \lambda, \Gamma, \mu, a, b\}^\circ = argmin(\|\varepsilon_{xx} - \varepsilon_f\|^2) \quad (8),$$

where $\{s_{max}, n_f, \Delta z, i_x, c, \lambda, \Gamma, \mu, a, b\}^\circ$ is the optimal set of parameters, which depends on the model used. This process allows the estimation of each argument, if they are independent of each other.

A constrained minimization procedure should be used to solve this problem [32]. While the values of the shape parameters are limited to their validity domains (Table I), the values of n_f depend on the parameters of the soil and the cable. We propose here to confine n_f to between 0 and 1, instead of 0.4 and 0.9 for *n* of (6). Also, the factor $|A(z)| = \frac{n_f \times s_{max}(z)}{\Delta z}$ is the combination of the coefficient that is influenced by the interface between the cable and the ground, the depth of the cavity, and the maximal vertical displacement of the ground. The value of this factor can be identified only if additional assumptions are introduced into the analysis. Although n_f can be assumed to be known (e.g., type of soil and cable, stiffness, and others), the depth of the underground cavity and the ground displacement have to be estimated. In tunneling applications, the depth of the man-made cavity is known, while in our context, the depth of the sinkhole is not known; only the ratio between the maximal vertical displacement and the depth can be determined. As minimizing a quadratic error cannot estimate each parameter separately, the next section proposes a methodology to estimate each parameter independently.

B. Methodology for vertical displacement estimation

The solution for the independent estimation of each parameter is the introduction of supplementary information between the researched parameters and the shape of the displacement. The depth is assumed to be proportional to the longitudinal extension of the displacement signature, and the soil/ cable parameter is assumed to be independent of the observation depth.

1) Sinkhole depth estimation

It is commonly assumed that the longitudinal extension, i_x, of the modeled strain profile is related to the depth of the cavity, z_s [33]-[34], and is expressed as:

$$i_x(z) = \alpha \times (z - z_s) = \theta + \alpha \times z \quad (9),$$

where α is a dimensionless constant that ranges from 0 to 1, depending on the soil type. In consequence, the value of i_x evolves within the observation depth, z_s, with a slope of $\alpha = \frac{\partial i_x}{\partial z_s}$ and a *y*-intercept of $\theta = -\alpha \times z_s$.

Empirically, α can be estimated from laboratory tests on different kinds of soil. However, because of the scaling issue and the possible heterogeneity of the soil in industrial structures, the field value of α might differ from that estimated in the laboratory. Therefore, the first problem here is the determination of α under field conditions. From (9), i_x is linearly dependent on the difference between the cavity depth, z_s, and the observation depth, *z*. We thus propose to monitor the structure at $Z \geq 2$ observation depths with several optical fiber cables [35]. This configuration allows *Z* strain measurements of the same event to be obtained. The confrontation of each strain measurement with the state-of-the-art models (Table I) or with the proposed model of (1) allows the estimation of the longitudinal extension, $i_x(z)$, for each observation depth, $z \in [1, Z]$, as shown in Fig. 2a.

This configuration allows the experimental determination of the evolution of i_x depending on the observation depth, *z*. Then, fitting a linear curve to the *Z* points, it is possible to estimate the coefficient $\tilde{\alpha} = \frac{\partial i_x}{\partial z}$. As a consequence, the sinkhole depth is $|z_s| = \frac{\tilde{\theta}}{\tilde{\alpha}}$. Logically, the more important *Z* is, the more the uncertainty on z_s will decrease.

2) Vertical displacement estimation

The following step is devoted to the assessment of the soil/ cable parameter n_f. To correctly estimate this value, we propose some recommendations. As n_f depends on the cable constitution, the same fiber optic cable should be used at different depths. The properties of the soil, in terms of its stiffness, granularity, and water content, must be constant,

depending on the x-axis, depth and time. With these hypotheses, n_f is considered to be constant on the x-axis and z-axis. According to the vertical maximal displacement, the depth of the cavity can evolve depending on time, where n_f is the only parameter of the factor $A(z)$ that is constant over time t. This constant can be estimated through the following method.
When there are *T* strain profiles over time at several observation depths, *Z*, by minimizing the difference between *A(z,t)* and the minima *m(z,t)* (Fig. 2b), n_f can be found as the constant that satisfies the following condition:

$$n_f{}^{\circ} = \underset{0<n_f\leq 1}{\operatorname{argmin}}\left(\sum_{t=1}^{T}\sum_{z=1}^{Z}|A(z,t)-m(z,t)|^2\right) \quad (10).$$

Finally, the evolution of the maximal vertical displacement $s_{max}(z,t)$ depending on depth *z* and time *t* can be found at each observation depth, *z*, through the following expression:

$$s_{max}(z,t) = \frac{m(z,t)\times\Delta z(t)}{n_f{}^{\circ}} \quad (11).$$

A consequence of this method is the possible local solution for the optimization of *n*. The solution greatly depends on its initial value and the gradient descent algorithm might not find a global minimum. To test the stability of this solution, optimization can be iterated with several initial values. This method will give us the most likely estimation of *n*, depending on the number of iterations and the range of the initial values.

For comparison purposes, we use a reference displacement sensor placed above the cavity center at $x = x_s$ and at a same depth, *z*. This sensor provides the evolution that depends on the time of the maximal vertical displacement measurement, *u(z,t)*, at the same observation depth, *z*, and it is equal to $s_{max}(z, t)$:

$$\widetilde{n_f} = \frac{m(z,t)\times\Delta z(t)}{u(z,t)} \quad (12).$$

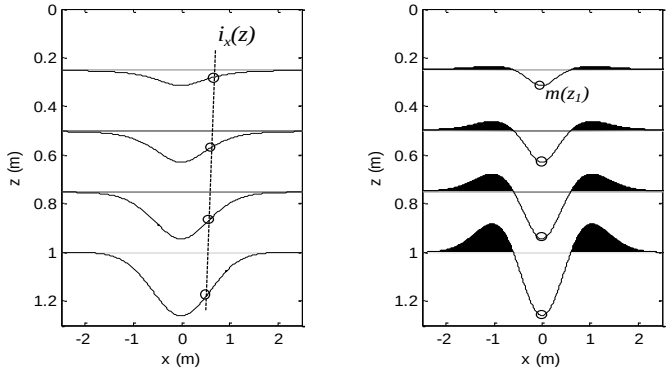

(a) (b)

Fig. 2. Simulation of the $Z = 4$ signatures for the displacement (a) and strain (b), considering the model based on (1), and depending on observation depths, *z*, and distance, *x*, and assuming z_s = 2 m, n_f = 0.5, and that $s_{max}(z)$ decreases linearly depending on *z*. $i_x(z)$ represents the longitudinal extension of the ground settlement. The signatures are rescaled and their positive areas are colored in black.

IV. Field Results and Discussion

In this section, we analyze the match between the displacement models and the strain measurements, and we present the application of the proposed methodology to estimate the vertical displacement.

A. Trap-door system and dataset

Centrifuge and trap-door systems are widely used to reproduce tunnel and sinkhole effects in the natural structure of the soil [27]-[36]. A trap-door experiment proposed by Blairon *et al.* [17] is schematized in Fig. 3a; this created vertical displacement on a column of granular material above a metal plate of 1 m in length. Three steps lead to the creation of an artificial sinkhole: the soil follows the displacement of the plate, and then the arching effect creates an underground cavity above the plate, and, finally, the mechanism of failure of the cavity leads to the sinkhole [36]. The depth of the cavity is chosen as 1.5 m corresponding to the classical depth reached by a digging engine. It is meant to represent a trench in a dyke. As shown in [37], the movement of the trap is transmitted to the surface of the soil if the ratio between the size of the trap and the depth of the cavity is below 1. This relation also depends on the soil density and the type of soil. This condition is not respected in our study but it is meant to be representative of the field conditions.

The ground settlement, E_p, is generated using a hydraulically controlled actuator that moves the plate. In this experiment, the index of the number of trap displacements, $p \in \{1,..,P\}$, with $P = 7$, evolved from E_1 = 2 mm to E_7 = 29 mm. To measure the vertical displacement in soil, two vertical local displacements sensors (LDS) were installed at two observation depths: z_1 = 0.5 m and z_2 = 1.0 m, from the surface (their instrumental uncertainties were +/-0.1 mm), to limit the influence of the edge effects near the surface and the trap. These vertical sensors measure the length of a wire between a fixed point beneath the trap and the observation depth.

The strain sensors were composed of two interrogators: an OBR 1600 Rayleigh scattering device (Luna Technology), and a Brillouin scattering device (DiTest STA-R; Omnisens). These interrogators provide strain measurements with spatial resolution of 3 cm and 40 cm, respectively. They were coupled to an optical fiber cable that was laid at the same observation depths as the LDS (z_1 = 0.5 m, z_2 = 1.0 m, from the surface). The optical cable is an industrialized cable made of a polymer coating.

The measured strain signatures provided by the Rayleigh device are shown in Fig. 3b. At E_1 = 2 mm, the vertical displacement measured by LDS reveals that the ground settlement is of the order of 0.1 mm (±0.1 mm) and 0.7 mm (±0.1 mm) at z_1 = 0.5 m and z_2 = 1.0 m, respectively. The strain minima are $m(z_1,E_1)$ = -165 µm/m and $m(z_2,E_1)$ = -244 µm/m, respectively. The Rayleigh-based sensor is thus sensitive enough to detect submillimeter ground settlement (Fig. 3b).

In the following, we will analyze the fitting of each displacement model with the Rayleigh strain measurements. These measurements are more accurate than those provided by the B-OTDA, and so they allow the choice of the best model

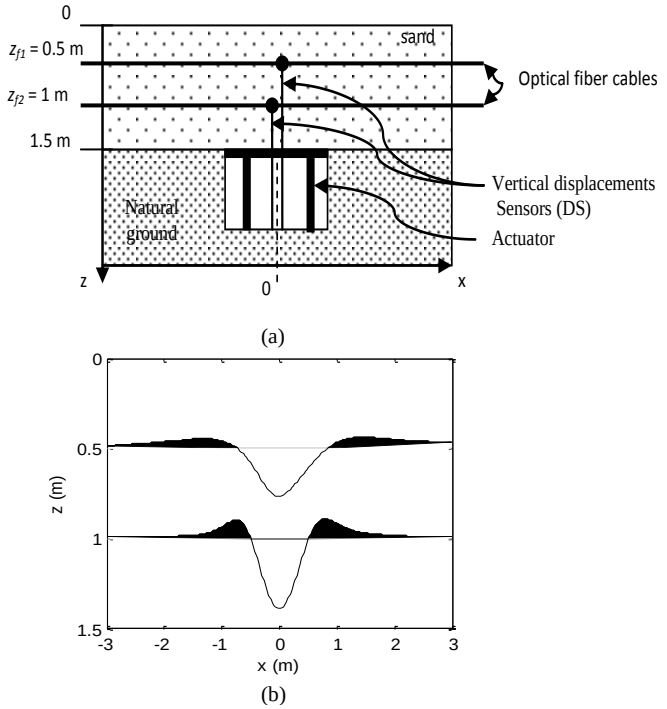

Fig. 3. (a) Illustration of the trap-door experiment: two cables and vertical displacements sensors are installed at two observation depths z_1 = 0.5 m and z_2 = 1.0 m from the surface of the sand. (b) Strain measurements at z_1 = 0.5 m and z_2 = 1.0 m provided by the OBR 1600 Rayleigh scattering device for ground settlement generated by a plate with E_1 = 2 mm. The signatures are rescaled and their positive areas are in black.

to calculate the shape parameter, i_x. As the strain shape the first step in the displacement quantification is the estimation of the depth of the sinkhole. Then, the estimation of the coefficient n_f allows the determination of the vertical displacement. The comparison with the reference displacement measurements (using LDS) is discussed.

B. Comparison of models

The choice of the model which best matches the shape of the strain measurements is a crucial step in the estimation of the inflexion point, i_x (9). Minimizing the quadratic error between the model and strain measurements according to (8) allows the parameters that are needed to quantify the displacement to be found. Consequently, the best performing model has to be chosen to fit the strain measurements. We thus compare the four state-of-the-art models (Table I) and the proposed model (based on (1)) with the strain signatures at both observation depths, z_1 and z_2, as shown in Fig. 3b. For quantitative comparison, we focus only on the matching distributions defined as the mean of the absolute error (*AE*) between the strain measurement $\varepsilon_f^{E_p}(x, z, E_p)$ for the trap displacements *p* and model *j*, with j = {G, C, J, V, B}, as the models for the longitudinal strain profile (i.e., Gaussian, Celestino, Jacobsz, Vorster, and based on (1), respectively).

$$AE^j(z) = 1/P \times \sum_{p=1}^{P} \sum_x \left| \varepsilon_f^{E_p}(x,z) - \varepsilon_{xx}^j(x,z) \right| \qquad (13).$$

We chose a box plot representation to compare the $AE^j(z)$ distributions according to the models and trap displacement

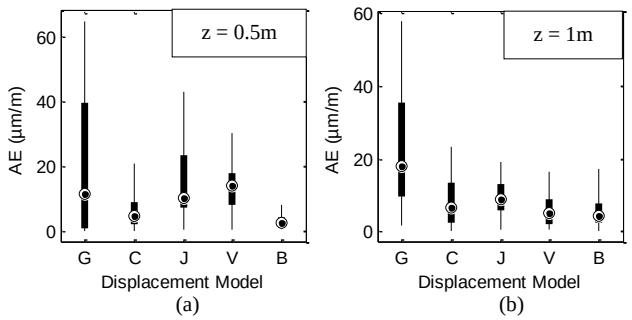

Fig. 4. Box plots of the means of the absolute errors between the modeled strain profiles and the Rayleigh strain measurements, for the several curves based on equations in Table I : Gauss (G), Celestino (C), Jacobsz (J), Vorster (V), and the curves based on (1), for each observation depth z_1 = 0.5 m (a) and z_2 = 1.0 m (b). The median of the distribution is marked as a point.

(Fig. 4). For each box plot, the median of the distribution is marked as a point, 50% of the error distribution is contained in the box, and the rest in the whiskers. Therefore, the best model must not show spread around the median, which should be near 0.

Based on these results, the Gaussian curve model (Fig. 4, G) does not fit the strain measurements for either observation depth: the *AE* is spread with a maximum error of around 60 µm/m and has an asymmetric distribution with most of the errors greater than the median (11 µm/m for z_1 = 0.5 m, 18 µm/m for z_2 = 1.0 m). The Celestino model (Fig. 4, C) provides the best fit with the strain distribution among the state-of-the-art models, because of the three degrees of freedom for the shape (Table I).

However, we note that for z_1 = 1 m, the Vorster model (Fig. 4, V) shows a better error distribution than the Celestino and Jacobsz (Fig. 4, J) models. Contrary to those models, the proposed model based on (1) provides correct fits for the strain measurements at both depths. The median error here (4.5 µm/m for z_1 = 0.5 m; 2.5 µm/m for z_2 = 1.0 m) reaches the minimum among all of the median errors at both depths, and the dispersion is the narrowest across all of these models. The proposed model, which mixes a Gaussian function with a.Lorentzian one, allows more signatures to be covered and exactly fits the strain measurements induced by the vertical displacement in this experiment

C. Sub-millimetric vertical displacement estimation

1) Depth and vertical displacement estimation using the Rayleigh strain measurements

As the proposed model (based on (1)) provides the best fit for the measured strain profiles at both depths, it is used to determine the sinkhole depth, z_s. The inflexion points $i_x(z,E_p)$ are found through the zeros of $\frac{\partial^2 u_z(x,z)}{\partial^2 x}$. As the two observation depths are well enough spaced on the z-axis, the modeled strain profiles have two different shapes.

It is thus possible to estimate $\tilde{\alpha}(E_p)$ as the slope of $i_x(z,E_p)$, and then $z_s(E_p)$ (see (9)). For the ground settlement E_1 = 2 mm we obtain $z_s(E_1)$ = 1.75 m, which is in the range of the depth of the trap-door system. If the two observation depths were too close, the different strain profiles would have been roughly similar and this estimation would not be interpretable. More the cables are spaced from each other, more the estimation will be improved, because the slope estimation would be more precise.

The evolution of the relative depth ($z_s(E_p)$ - z_s (E_1)) that depends on the trap displacement shows that the center of the sinkhole exponentially decreased by about 10 cm (Fig. 5a). Unfortunately, no other sensors were installed to measure the loss of granular particles through the trap door to validate this assessment, but the estimated vertical displacement and the measured vertical displacement by LDS will be compared to validate the proposed methodology.

As the depth cavity has been estimated, the next step is estimation of the interface cable/ soil coefficient n_f. The initial value was fixed based on the literature, which indicates that in unsaturated sandy soil, n_f should approach 0.4. We iterate the process (see (10)) to compare the solutions with several initial values of n_f° around 0.4 ±0.1. This approach allows the most likely value to be found, which is n_f° = 0.36, from 92% of the iterations. As a comparison with this value, the second way to estimate this is to use the LDS measurements (see (12)). The $\tilde{n}_f$ calculated using (12) for z_1 = 0.5 m, E_1 = 2 mm is within the same approximate size: $\widetilde{n_f} = 0.32$. Under real conditions, the latest solution had the constraint of the installation of a vertical displacement sensor in the structure that was parallel to the optical fiber. We show hereafter that the optimization approach avoids such a problem and enables the approximation of the interface cable/ soil coefficient. This method is thus chosen for the following sections.

Finally, the maximal vertical displacement calculated through (10) is shown in Fig. 5b. According to LDS, the sand column above the trap moves slightly, from 0.1 mm (±0.1 mm) to 0.2 mm (±0.1 mm) at z_1 = 0.5 m, and from 0.7 mm (±0.1 mm) to 1.1 mm (±0.1 mm) at z_2 = 1.0 m, (Fig. 5.b).We can see that at each depth, s_{max} exactly follows this trend and is contained in the instrumental uncertainties of the LDS sensors. These results validate the assumptions made previously, with the proposed methodology validated using the strain profiles measured by a Rayleigh scattering-based device. Therefore, with this methodology, it is possible to estimate sub-millimeter displacement from DOFS measurements.

For dyke monitoring, a trench is dug through the structure and the optical fiber cables should be installed, as we recommend in this article, parallel to the surface. The soil between cables has to be uniform. However, in others applications, these conditions might not been verified. If the soil is not uniform, the measured strain signatures will not be coherent with each other and the displacement model will not fit data. As a consequence, the displacement estimation will be inaccurate and only the detection of a movement could be given by the measurement system. If the cables are not parallel to the surface, the 2D model proposed in this article has to be extended to a 3D model.

2) Estimation of the vertical displacement using B-OTDA strain measurements

As the Rayleigh device monitoring length is limited to 100-m, we study here the possibility to use an industrial B-OTDA device to estimate the vertical displacement according to the same methodology. The B-OTDA device performs strain profiles with 40-cm spatial resolution, instead of the centimeter spatial resolution provided by a Rayleigh device. As the spatial extension of the strain signature induced by the sinkhole is

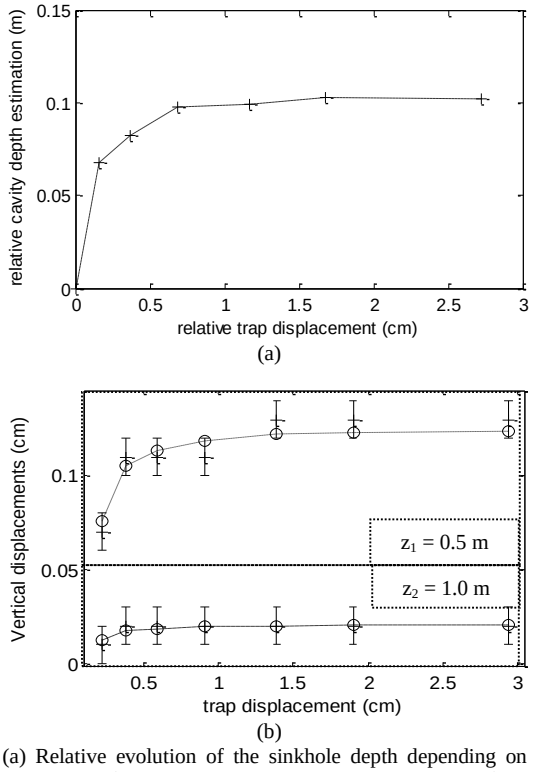

Fig. 5. (a) Relative evolution of the sinkhole depth depending on the trap displacement. The reference depth is z_s = 1.75 m. (b) Estimation of the maximal vertical displacement $s_{max}(z,E_p)$ (with n_f° = 0.36) using the proposed model (based on (1)) and the Rayleigh strain measurements, depending on the trap displacement for both observation depths z_1 = 0.5 m (top, circles) and z_2 = 1.0 m (bottom, circles). Comparison with the LDS displacement measurements $u(z,Ep)$ (crosses) and the associated uncertainty errors are shown.

around 2 m, and as the raw B-OTDA strain subsample profile is compared to the Rayleigh one, the strain signature is not accurate (Fig. 6): the minima are -180 µm/m at z_1 and -280 µm/m at z_2, instead of -255 µm/m and -420 µm/m, respectively, for the Rayleigh strain measurement. As a consequence, the assumption of (4) that the system of interrogation does not interact with the strain profile is not respected, and the estimation of s_{max} might be inaccurate. A post-processing methodology is now applied that was proposed recently [14] and that allows estimation of a strain profile from the raw spectral data of the Brillouin sensor with 5-cm spatial resolution. This methodology provides a strain profile (Fig. 6, solid line) that has better strain resolution than the raw strain provided by the industrial B-OTDA device (Fig. 6, crosses).

Compared to the Rayleigh strain measurements (Fig. 6, dotted line), the post-processed B-OTDA strain profile is perfectly estimated at z_1. In terms of error between the Rayleigh profile and the post-processed B-OTDA strain profile, the mean square error is around 0.5%.

At z_2 the profile is slightly asymmetric and noisier, and the mean square error is higher, at ~2%. However, this approach provides better reconstruction of the strain signature than the raw data provided by the industrial B-OTDA device. Indeed, the minima of the strain are around $\tilde{m}(z_1,E_3)$ = -254 µm/m and $\tilde{m}(z_2,E_3)$ = -388 µm/m.

The estimation of the displacement is applied to the post-processed B-OTDA strain profiles using the proposed model based on (1). The first step is the determination of the shape parameter of the pseudo-Voigt model (see (1)) through (8).

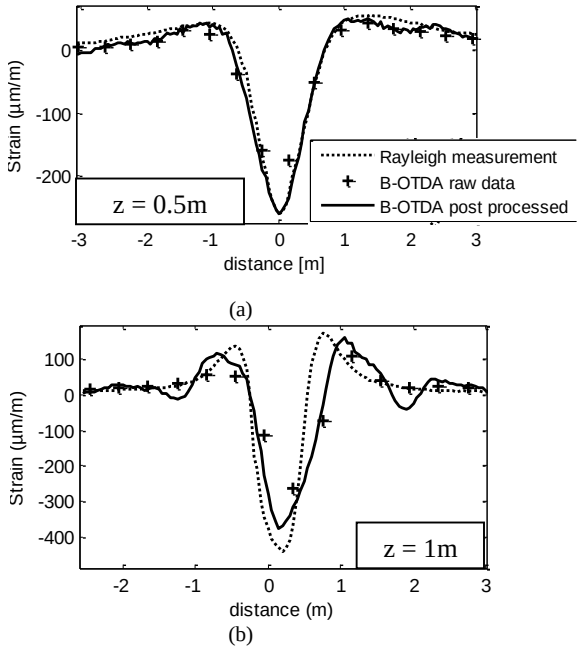

Fig. 6. Post-processed strain profile from raw B-OTDA spectral data with a spatial resolution of 5 cm (solid line). Comparison with the raw data provided by the industrial B-OTDA device (+) and the Rayleigh strain measurements (dotted line), with spatial resolutions of 40 cm and 3 cm, respectively, for both of the depth observations of z_1 = 0.5 m (a) and z_2 = 1.0 m (b), for E_3 = 0.6 mm.

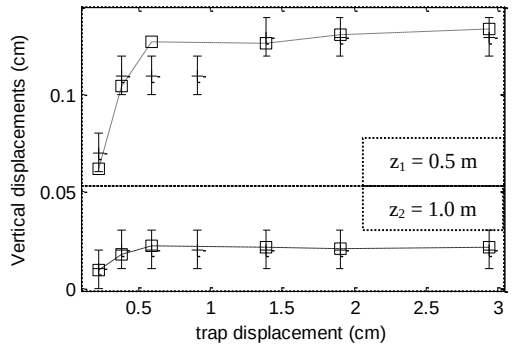

Fig. 7. Estimation of the maximal vertical displacement $s_{max}(z,E_p)$ with (n_f° = 0.2) using the proposed model (based on (1)) and the post-processed B-OTDA strain measurements, according to the trap displacement for both of the observation depths z_1 = 0.5 m (top, squares) and z_2 = 1.0 m (bottom, squares). Comparisons with the LDS displacement measurements $u(z,E_p)$ (crosses) and the associated uncertainty errors are shown.

As the post-processed profiles are relatively noisy compared to the Rayleigh profiles, the fitting errors between the post-processed B-OTDA strain profiles and the modeled strain profiles are greater, although they remain satisfying: the median *AE* is 15 µm/m for z_1, and 30 µm/m for z_2.

As the post-processed strain profile is larger than the Rayleigh profile at z_2 (Fig. 6b), the i_x calculated from the modeled strain profile is greater, while at z_1, it has the same value because the post-processed strain profile is better estimated. As a consequence, the value of the slope α is smaller. This decrease is of the order of 3%, and it is constant for all of the ground settlement, E_p. The estimation of the sinkhole depth suffers from this effect, as its value changes from 1.75 m to 2.0 m.

This is the first time that sub-millimeter displacement estimation has reached such precision. This shows that the use of the post-processed technique is crucial to provide accurate strain profiles from B-OTDA devices. With this methodology coupled with a B-OTDA, this enables the estimation of the ground settlement with great accuracy compared to the LDS. New sensors techniques are in development or industrialized as the combined Rayleigh-Brillouin sensor [38] which provides strain measurements with centimeter spatial resolution over kilometers of optical fiber. The proposed methodology used on those measurement should provided precise estimation, as good as the results obtained with the Rayleigh device.

V. Conclusion

The problem of the quantification of displacement in large soil structures, such as dams, using DOFS has been addressed here. These sensors provide strain measurements in the longitudinal axis of the optical fiber. Careful interpretation of the strain signatures is crucial for the retrieval of the vertical displacement. The relation between the longitudinal strain profile measured by DOFS and the ground displacement profile is based on four parameters: a coefficient influenced by the interface of the soil and the optical fiber cable; the spatial extension of the ground-settlement profile; the depth of the sinkhole; and the vertical displacement induced. Through the strain measurements and the model, it is possible to estimate the displacement in the soil according to some given assumptions.

A methodology has been proposed to independently estimate the vertical displacement in the structure from the other parameters. The main idea is to consider the same optical fiber cable at several observation depths above the sinkhole. The property of the granular material between the several depths must be continuous. For the same displacement in the soil, the DOFS allows the measurement of several strain profiles at different depths, to provide modeled strain profiles of the same event. Therefore, the depth of the cavity can be estimated through the evolution of the spatial extension of the ground settlement.

To validate this methodology, an experiment was carried out under controlled conditions to create a sinkhole in a sandy soil structure. One optical fiber cable was spaced at 50 cm at two different observation depths. The optical fiber cable was coupled with Rayleigh and Brillouin scatter devices. The methodology was applied to the strain measurements provided by the Rayleigh device and to the post-processed Brillouin strain profiles, to estimate the vertical displacement. These estimates were validated by the LDS. This experiment shows that the proposed methodology and installation devices can detect, localize, and quantify sub-millimeter vertical displacement with high precision.

Further studies are planned to confront this new empirical model with an analytical model under two-dimensional conditions. The generalization of the model under three-dimensional conditions can also be addressed. Under field conditions, the sinkhole does not necessarily appear in the same plane as the optical fiber. The three-dimensional model would enable the study of the influence of the position of a sinkhole on the strain signature. The solution to detect, localize, and quantify ground settlement in industrialized structures would be the installation of the same cable along several planes of the structures. It would then be interesting to establish the ability of this mesh of cables to estimate the ground settlement and its

origin in terms of the distances between the cables. It would also be interesting to study the influence of the type of optical fiber cable on the estimation of the vertical displacement. Such a study would lead to the choice of the most compatible cable, taking into account the ground properties.

REFERENCES

[1] Fry, J. J., (1997). "Internal erosion and surveillance." 19th Annual Meeting of the International Commission on Large Dams Congress, Florence.

[2] Vogel, B., Cassens, C., Graupner, A., and Trostel, A., (2001) "Leakage detection systems by using distributed fiber optical temperature measurements," *Proc. SPIE*, Vol. 4328, pp. 23-34, January.

[3] Johansson S., and Sjodahl, P., (2004), "Downstream seepage detection using temperature measurements and visual inspection monitoring experiences from Røsvatn field test dam and large embankment dams in Sweden," in *Proc.Int. Seminar Stability Breaching Embankment Dams*, pp. 1-21.

[4] Rozycki, A., Ruiz, J. M., and Caudra, A., (2005). "Detection and evaluation of horizontal fractures in earth dams using the self-potential method," *Eng. Geol.*, Vol. 82, No. 3, pp. 145-153, January.

[5] Sjodahl, P., Dahlinb, T., Johansson, S., and Lokec, M. H., (2008) "Resistivity monitoring for leakage and internal erosion detection at Hällby embankment dam," *Journal of Applied Geophysics*, Vol. 65, Nos. 3-4, pp. 155-164, September.

[6] Wade, S. A., Grattan, K. T., and McKinley, B., (2004). "Incorporation of fiber-optic sensors in concrete specimens: Testing and evaluation." *IEEE Sensors Journal*, Vol. 4, No. 1, pp. 127–134.

[7] Hénault, J.M., Quiertant, M., Delepine-Lesoille, S., Salin, J., Moreau, G., Taillade, F., and Benzarti, K., (2012) "Quantitative strain measurement and crack detection in RC structures using a truly distributed fiber optic sensing system". *Construction and Building Materials*, Vol. 37, pp. 916–923.

[8] Bastianini, F., Rizzo, A., Galati, N., Deza, U. and Nanni, A. (2005, May). "Discontinuous Brillouin strain monitoring of small concrete bridges: comparison between near-to-surface and smart FRP fiber installation techniques". *In Proceeding of Smart Structures and Materials, International Society for Optics and Photonics*, Vol. 5765, pp. 612-623.

[9] Klar, A., and R. Linker, (2010). "Feasibility study of automated detection of tunnel excavation by Brillouin optical time domain reflectometry". *Tunnelling and Underground Space Technology*, Vol. *25*, No. 5, pp. 575-586.

[10] Khan, A. A., Vrabie, V., Mars, J. I., Girard, A., and D'Urso, G., (2008) "A source separation technique for processing of thermometric data from fiber-optic DTS measurements for water leakage identification in dikes" in *IEEE Sensors Journal*, vol. 8, no. 7, pp. 1118–1129.

[11]Khan, A.A.; Vrabie, V.; Mars, J.I.; Girard, A.; d'Urso, G., (2010) "Automatic Monitoring System for Singularity Detection in Dikes By DTS Data Measurement," , *IEEE Transactions on Instrumentation and Measurement*, Vol.59, No.8, pp.2167-2175.

[12] Mars J.I., Buchoud, E., Vrabie, V., Khan, A. A., Blairon, S. and D'urso, G., (2013), "Source separation and distributed sensing: The key of an efficient monitoring", *5th International Workshop on Computational Advances in Multi-Sensor Adaptive Processing, San Martin*, French West Indies, 15-18 December 2013, pp 264-267.

[13] Buchoud, E., Vrabie, V., D'Urso, G., Henault, J-M., Girard, A., Mars, J.I., and Blairon, S., (2014). "Parametric inversion of Brillouin spectra using L-curve criterion to enhance the accuracy of distributed strain measurement". *76th European Association of Geosciences Engineering Conference and Exhibition*, Amsterdam, Netherlands, 16-19 June.

[14] Hartog, A. H. (2002), "Progress in distributed fiber-optic temperature sensing." Proc. SPIE, Fiber Optic Sensor Technology and Applications, Vol. 4578, pp. 43–45.

[15] Soller B. J., Gifford, D., Wolfe, M., and Froggatt, M., (2005) "High resolution optical frequency domain reflectometry for characterization of components and assemblies", *Optics Express*, Vol. 13, pp. 66-674.

[16] Bao, X., and Chen, L., (2011). "Recent progress in Brillouin scattering based on fiber sensors," in *Sensors*, Vol.11, pp. 4152–4187.

[17] Blairon, S., Hénault, J-M., Buchoud, E., Vinceslas, G., and Delepine-Lesoille, S., (2011) "Truly distributed optical fiber extensometers for geotechnical structure monitoring (dikes and underground repository): Influence of sensor external coating" *8th International Symposium of Field Measurements of Geomechanics*, Berlin, Germany, September.

[18] Ravet F., Ortiz, E.G., Peterson, B., Hoglund, G., and Nikles, M., (2011) "Geohazard prevention with online continuous fiber optic monitoring", at *Rio Pipeline Conference and Exposition*, Septembre, Rio, Brazil.

[19] Rochat E., and Nikles, M., (2014). "Enhanced Brillouin distributed strain and temperature sensing for structural health monitoring in industrial applications", 7th European workshop on Structural Health Monitoring, Nantes, France, July 8-11.

[20] Mamdem, Y. S., Burov, E., de Montmorillon, L. A., Jaouën, Y., Moreau, G., Gabet, R., and Taillade, F. (2012). "Importance of residual stresses in the Brillouin gain spectrum of single mode optical fibers". *Optics express*, Vol. 20, No. 2, pp. 1790-1797.

[22] Peck, R. B. (1969). "Deep excavations and tunnelling in soft ground". Proceeding of 7th Int. Conference of Soil Mechanics Foundation Engineering, Mexico City, pp. 225–290.

[22] Bobet, A. (2001). "Analytical solutions for shallow tunnels in saturated ground". *Journal of Engineering Mechanics*, Vol. 127 No. 12, pp. 1258-1266.

[23] Klar, A., Dromy, I., and Linker, R., (2014). "Monitoring tunneling induced ground displacements using distributed fiber-optic sensing". *Tunnelling and Underground Space Technology*, Vol. 40, pp. 141-150.

[24] Celestino, T. B., Gomes, R. A. M. P. and Bortolucci, A. A. (2000). "Errors in ground distortions due to settlement trough adjustment". In *Tunneling and Undergroung Space Technology*, Vol. 15, No. 1, pp. 97–100.

[25] Vorster, T. E., Klar, A., Soga, K., and Mair, R. J., (2005). "Estimating the effects of tunneling on existing pipelines". *In Journal of Geotechnical and Geoenvironmental Engineering*, Vol. 11, No. 131, pp. 1399-1410.

[26] Jacobsz, S. W., Standing, J. R., Mair, R. J., Hagiwara, T. and Sugiyama, T. (2004). "Centrifuge modelling of tunnelling near driven piles". *Soils Foundation*. Vol. 44, No. 1, pp. 49–56.

[27] Marshall, A., Farrell, M. R., Klar, A., and Mair, R., (2012), "Tunnels in sand: the effect of size, depth and volume loss on Greenfield displacements", in *Géotechnique*, Vol. 62, No. 5, pp. 385-399.

[28] Bao, X., J. Dhliwayo, N. Heron, D. J. Webb, and Jackson, D. A., (1995). "Experimental and theorical studies on a distributed temperature sensor based on Brillouin scattering," in *Journal of Lightwave Technology*, Vol. 13, No.7, pp. 1340–1348.

[29] Ansari, F., and Libo, Y. (1998). "Mechanics of bond and interface shear transfer in optical fiber sensors". *Journal of Engineering Mechanics*, Vol. 124, No. 4, pp. 385-394.

[30] Klar, A., Bennett, P. J., Soga, K., Mair, R. J., Tester, P., Fernie, R., and Torp-Peterson, G. (2006). "Distributed strain measurement for pile foundations". In *Proceedings of the ICE-Geotechnical Engineering*, Vol.159, No. 3, pp. 135-144.

[31] Attewell, P. B., Yeates, J., and Selby, A. R. (1986). "Soil movements induced by tunnelling and their effects on pipelines and structures". Blackie.

[32] Byrd, R.H., J. C. Gilbert, and Nocedal, J., (2000) "A Trust Region Method Based on Interior Point Techniques for Nonlinear Programming," *Mathematical Programming*, Vol 89, No. 1, pp. 149–185.

[33] O'Reilly, M. P. and New, B. M. (1982). "Settlements above tunnels in the United Kingdom: their magnitude and prediction". Proceedings Tunnelling '82, Brighton, pp. 173–181.

[34] Mair, R. J., R. N. Taylor, and Bracegirdle, A., (1993), "Subsurface settlement profiles above tunnels in clays", in *Géotechnique*, Vol. 43, No. 2, pp. 315-320.

[35] Buchoud, E., Mars, J., Blairon, S., and D'Urso, G. (2014). "Procédé et dispositif pour la détermination de la profondeur de l'origine d'un tassement de sol", French patent FR 14/57690.

[36] Meguid, M. A., Saada, O., Nunes, M. A., and Mattar, J. (2008). "Physical modeling of tunnels in soft ground: a review". *Tunnelling and Underground Space Technology*, Vol. 23, No. 2, pp. 185-198.

[37] Santichaianaint, K. (2002). "Centrifuge modeling and analysis of active trapdoor in sand." Ph.D. thesis. Dept. of Civil, Environmental and Architectural Engineering, Univ. of Colorado at Boulder.

[38] Yamauchi (2010) "A measurement method to determine strain and temperature coefficients in fiber optic sensors," *presented at Proc. of Asian Pacific Workshop on Structural Health Monitoring Conference*, Tokyo, Japan.